

CFA-15 – a perfluorinated metal–organic framework with linear 1-D Cull-chains containing accessible unsaturated, reactive metal centres

Julia Fritzsche, Romy Ettlinger, Maciej Grzywa, Stephan G. Jantz, Andreas Kalytta-Mewes, Hana Bunzen, Henning A. Höppe, Dirk Volkmer

Angaben zur Veröffentlichung / Publication details:

Fritzsche, Julia, Romy Ettlinger, Maciej Grzywa, Stephan G. Jantz, Andreas Kalytta-Mewes, Hana Bunzen, Henning A. Höppe, and Dirk Volkmer. 2019. "CFA-15 – a perfluorinated metal–organic framework with linear 1-D Cull-chains containing accessible unsaturated, reactive metal centres." *Dalton Transactions* 48 (40): 15236–46.
<https://doi.org/10.1039/c9dt02133g>.

Nutzungsbedingungen / Terms of use:

licgercopyright

Dieses Dokument wird unter folgenden Bedingungen zur Verfügung gestellt: / This document is made available under these conditions:






Deutsches Urheberrecht

Weitere Informationen finden Sie unter: / For more information see:

<https://www.uni-augsburg.de/de/organisation/bibliothek/publizieren-zitieren-archivieren/publiz/>



CFA-15 – a perfluorinated metal–organic framework with linear 1-D Cu^{II}-chains containing accessible unsaturated, reactive metal centres†

J. Fritzsche,  R. Ettlinger, M. Grzywa,  S. G. Jantz, A. Kalytta-Mewes, H. Bunzen,  H. A. Höppe  and D. Volkmer *

The synthesis and crystal structure of the perfluorinated metal–organic framework **CFA-15** (Coordination Framework Augsburg University-15), Cu₃^{II}(tfpc)₂(OH)₂·DMF, as well as the crystal structure of its ligand (H₂-tfpc = 3,5-bis(trifluoromethyl)-1H-pyrazole-4-carboxylic acid) are described. The MOF crystallizes in the monoclinic crystal system within the chiral space group C2 (no. 5). It features a 3-D microporous framework with rhombic channels along the *c*-axis. The MOF is formed by 1-D chains of Cu(II) ions expanding in the *c*-direction, bridged by OH[−] groups, DMF molecules and tfpc^{2−} ligands. Two different Cu(II) species are located within the structure, bridged in a {Cu1–Cu1–Cu2–Cu1–Cu1–Cu2} mode. By thermal treatment, it was possible to remove coordinated solvent molecules and generate free accessible, unsaturated and reactive metal centres. The structure of activated **CFA-15** was refined *via* Rietveld method. DRIFT measurements, which were used to study adsorption of CO₂ and NO in the MOF, showed a formation of a stable **NO-CFA-15** complex. **CFA-15** was further characterized by thermogravimetric analysis, variable temperature powder X-ray diffraction measurements, IR spectroscopy, as well as photoluminescence and gas sorption measurements. The isosteric heats of adsorption for CO, CO₂, H₂ and O₂ were determined, and compared to DFT calculated sorption energies as well as to data reported in literature for similar materials.

Introduction

Replacing hydrogen atoms by fluorine atoms in a metal–organic framework leads to so-called FMOFs (fluorous metal–organic frameworks), a special group of the metal–organic framework family. While several partially fluorinated MOFs have been published, only a few fully or extensively fluorinated MOF structures can be found in the literature.^{1–3,4a,d}

Fluorine substituents are strongly electronegative. Therefore, a fluorination in the structure leads to dramatic changes in the physical and chemical properties of FMOFs compared to the non-fluorinated counterparts. As a consequence, FMOFs often show low surface energy and surface tension, enhanced thermal and chemical stability, good stability

against (self-)oxidation and photonic decomposition as well as strong hydrophobicity.^{4,5a} There are different ways to generate new FMOFs: the most common way is to use fluorinated ligands for MOF synthesis, which is also the method which we explored in our previous work.^{6,7,37} Further possibilities to generate FMOFs are, for example, the functionalization by inorganic fluorinated anions or the fluoro-functionalization *via* plasma-enhanced chemical vapour deposition.⁸

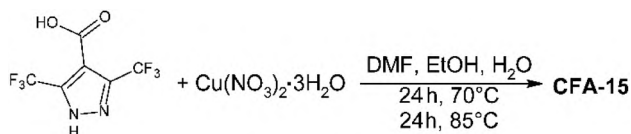
While the first fluorinated MOF was published in 2004⁹ and functionalized MOFs have become more and more important during the last few years, there are only two reviews about FMOFs so far and also the total number of publications is not rising dramatically.⁵ A possible reason for this could be the fact, that replacing hydrogen atoms by fluorine atoms often leads to unpredictable and unexpected coordination motifs within the MOFs instead of the expected topology observed within the non-fluorinated analogues. These unanticipated coordination geometries found in FMOFs could be due to steric hindrance stemming from the larger size of CF₃-groups compared to CH₃-groups or just simple hydrogen atoms.⁶

Whereas pyrazolate (pz) ligands with copper ions often result in the formation of polynuclear [Cu_{*n*}^I(pz)_{*m*}] units,^{7,10} carboxylate ligands usually favour a Cu(II) paddle-wheel secondary building unit.^{11,37} However, as mentioned above,

University of Augsburg, Institute of Physics, Chair of Solid State and Materials Chemistry, Universitätsstrasse 1, 86159 Augsburg, Germany.

E-mail: dirk.volkmer@physik.uni-augsburg.de; Fax: +49 (0)821 598 5955;

Tel: +49 (0)821 598 3006



Scheme 1 Synthesis of **CFA-15** from the H_2 -tfpc ligand and copper(II) nitrate.

replacing hydrogen atoms in linkers by fluorine atoms often leads to unexpected coordination units within the respective MOFs. In this work we used the fully fluorinated ligand 3,5-bis(trifluoromethyl)pyrazole-4-carboxylic acid (H_2 -tfpc) to prepare a Cu-MOF (Scheme 1). Within the structure of H_2 -tfpc, the total mass ratio of fluorine in the organic ligand is almost 50%. Therefore, it should not come as a surprise, that using the H_2 -tfpc ligand did not lead to a Cu-MOF which would be isostructural to the MOF prepared with the non-fluorinated analogue (3,5-dimethyl-4-carboxypyrazol).¹² Instead of that, 1-D chains of Cu(II) ions expanding in the c -direction and bridged by OH^- groups, DMF molecules and $tfpc^{2-}$ ligands were found. MOFs with such Cu(II) centres that are bridged with neutral solvent molecules as DMF or water can be found in literature.^{13–17} In some of these cases it has been possible to remove the solvent molecules by thermal treatment and to generate frameworks with coordinatively unsaturated metal centres. Such activated samples often represent promising candidates for gas separation, molecular sieving and purification applications. Therefore, we examined the possibilities to activate **CFA-15** and interactions of the activated sample with small gas molecules.

Results and discussion

Syntheses and characterisation

The ligand 3,5-bis(trifluoromethyl)pyrazole-4-carboxylic acid (H_2 -tfpc) was synthesized according to literature procedure.¹⁸ As there is no crystal data for the ligand so far, single crystals of H_2 -tfpc, obtained by slow evaporation of an aqueous solution, were analysed by X-ray diffraction and the results are discussed later in the article.

Blue block crystals of **CFA-15** framework (Fig. 1a–c) were obtained after heating a solution of H_2 -tfpc ligand and copper(II) nitrate trihydrate at 70 °C for one day and subsequently at 85 °C for further 24 h in a DMF/EtOH/ H_2O 1 : 1 : 1 mixture (Scheme 1).

Single crystal structure analysis

The ligand 3,5-bis(trifluoromethyl)pyrazole-4-carboxylic acid (H_2 -tfpc, $C_6H_2F_6N_2O_2$) crystallizes in the orthorhombic crystal system within the space group $Cmc2_1$ (no. 36). Detailed information on its crystal structure is presented in the ESI (Tables S4–S7 and Fig. S17, S18†).

CFA-15 crystallizes in the monoclinic crystal system within the chiral space group $C2$ (no. 5). The unit cell parameters are

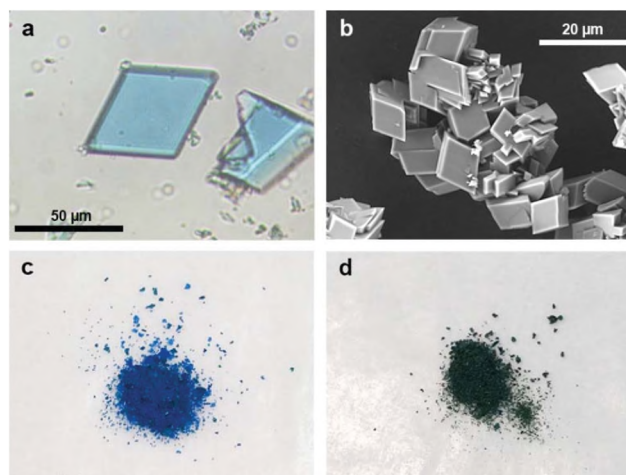


Fig. 1 **CFA-15**: (a) optical micrograph, (b) SEM image and (c) photo of a fresh synthesised powder sample, and (d) photo of an activated powder sample.

as follows: $a = 14.2997(4)$, $b = 9.4881(3)$, $c = 9.3862(3)$ Å, $\beta = 109.7120(10)^\circ$, $V = 1198.86(6)$ Å³. The asymmetric unit consists of two copper ions, one $tfpc^{2-}$ ligand, one DMF molecule and one OH^- group. An ORTEP-style plot of the asymmetric unit of **CFA-15** including atom labels, tables containing the atomic coordinates as well as isotropic thermal parameters, bond lengths and angles are presented in the ESI (Fig. S16 and Tables S1–S3†).

The structure of **CFA-15** exhibits two different Cu(II)-centres (see Fig. 2a). One Cu(II)-ion (Cu1) displays a square-pyramidal geometry (CuN_2O_3), with three chelating $tfpc^{2-}$ ligands and one OH^- group occupying the basal plane and one oxygen atom from a coordinated DMF molecule in the axial position. More precisely, Cu1 coordination geometry involves two nitrogen atoms stemming from two $tfpc^{2-}$ ligands, one oxygen atom from a third $tfpc^{2-}$ ligand, two oxygen atoms belonging to the OH^- group and to solvent molecules, respectively. The second Cu(II)-ion, namely Cu2, located on a special position (two-fold crystallographic axis, in Wyckoff notation $2a$) displays distorted planar square geometry (CuO_4). The Cu2 atom is coordinated by four oxygen atoms stemming from two $tfpc^{2-}$ ligands and two OH^- groups in trans-geometry. The structure of **CFA-15** exhibits asymmetrically heterobridged $[Cu_2(\mu-OR)(\mu-O_2C-R')]^{2+}$ cores, which can be found rarely in literature.¹⁹ Much more frequently, symmetrically bridged units are formed, as for example a $[Cu_2(\mu-O_2C-R)_4]$ paddle-wheel unit or doubly carboxylate-bridged $[Cu_2(\mu-O_2C-R)_2(L)]^{2+}$ (with L: neutral bi- or tridentate ligand).²⁰ The binuclear units are roof shaped with angles of about 124° between two basal planes. The $tfpc^{2-}$ ligands, OH^- groups and DMF molecules bridge the Cu(II)-ions in a mode $\{Cu1-Cu1-Cu2-Cu1-Cu1-Cu2\}$ along 1-D linear chains running parallel to the crystallographic axis c . Subsequently, the 1-D chains are connected by $tfpc^{2-}$ ligands creating a 3-D microporous non-interpenetrated framework with 1-D rhombic channels expanding along the c -direction of

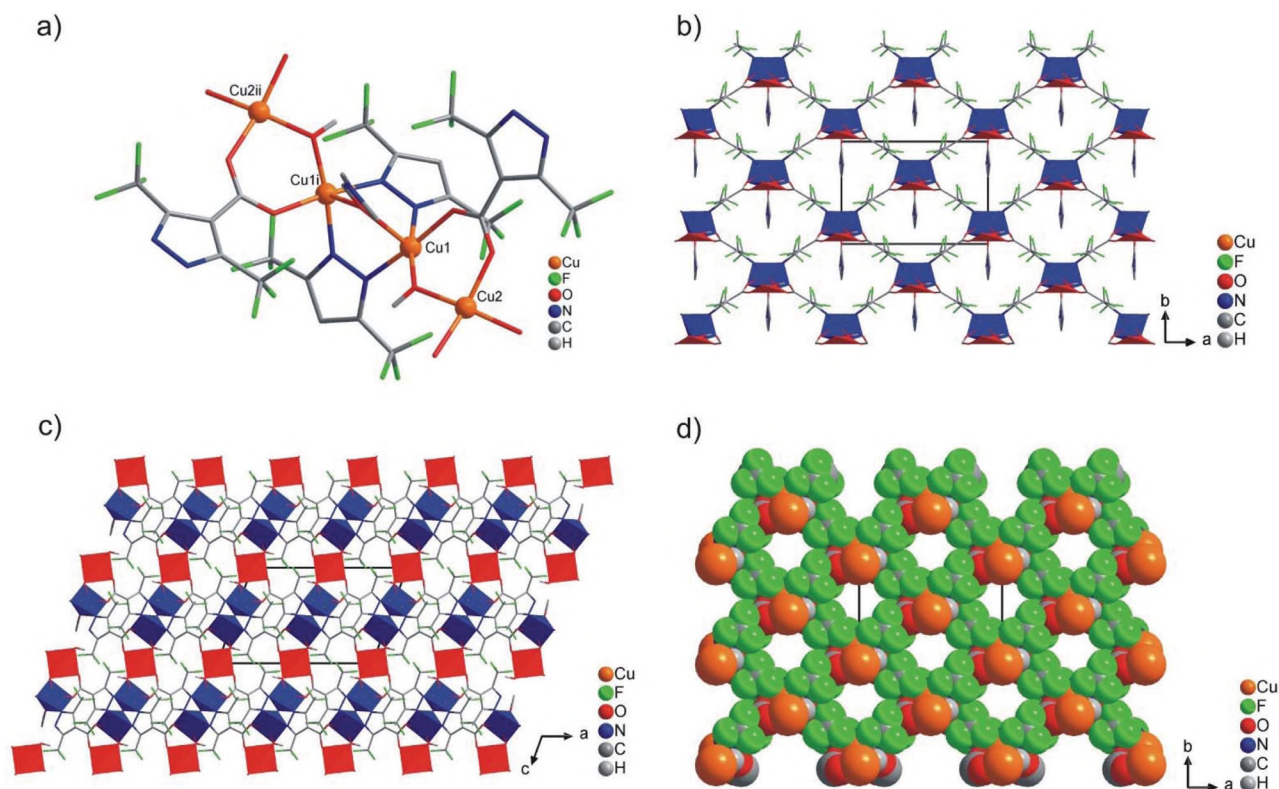


Fig. 2 Portion of the crystal structure of **CFA-15** emphasizing coordination of two Cu(II)-centres (a), Cu1i ($1 - x, y, 1 - z$), Cu2ii ($x, y, -1 + z$); packing diagram of the crystal structure of **CFA-15** viewed in *c*- (b) and *b*-direction (c); (d) portion of the crystal structure of **CFA-15** emphasizing channels, viewed in *c*-direction.

the crystal lattice (see Fig. 2b–d). The Cu–N and Cu–O distances range from 2.000(10)–2.035(10) and 1.876(9)–2.261(9). These values are in good agreement with those found in the structurally related Cu-MOFs.^{11a,21,37} The intramolecular Cu(1)···Cu(2) distance of 3.336 Å rules out any significant direct metal–metal contact. More exciting is a closer look on the Cu(1)···F distances within **CFA-15**: the smallest Cu(1)···F distance is 2.684 Å which is smaller than the sum of the van der Waals radii of copper and fluorine (Cu: 1.96 Å; F: 1.35 Å). This suggests the formation of weak bindings between the Cu(II) ions and the fluoro substituents of the ligand.

The DMF molecules bridging Cu1–Cu1 atoms are located on the two-fold crystallographic axis and are oriented towards the centre of the rhombic channels. Taking the van der Waals radii of fluorine atoms (1.35 Å) into account, the channel diameter calculated between the fluorine atoms is 4.2 Å. Estimation using the SQUEEZE software reveals that the initial solvent accessible void volume is 230.9 Å³, which is 19.3% of the unit cell volume (1198.9 Å³) for a probe radius of 1.68 Å, corresponding to the approximate van der Waals radius of argon.

Thermal analysis and VTXRPD studies

Thermal stability of **CFA-15** was investigated by thermogravimetric analysis (TGA) and variable temperature X-ray powder diffraction (VTXRPD) measurements. To remove the occluded solvent molecules, the sample was pre-dried in

vacuum at 100 °C for 4 h prior to TG measurements. As shown in Fig. 3, the pre-dried **CFA-15** sample shows no weight loss until 200 °C. The loss of coordinated DMF molecules can be observed by the weight loss step between 220–250 °C, which is not well resolved. Above this temperature, the framework rapidly decomposes.

Phase purity of **CFA-15** was confirmed by XRPD measurements at room temperature (Fig. 4). The experimental XRPD

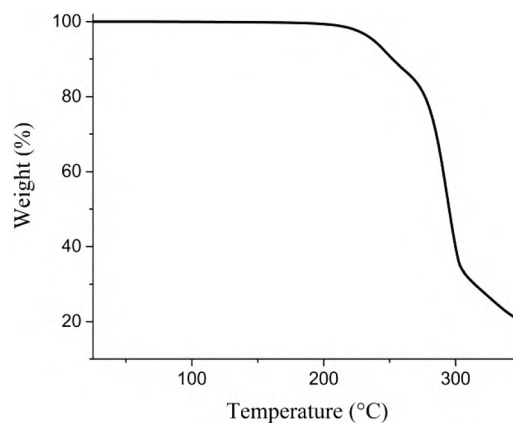


Fig. 3 Temperature dependent weight loss of **CFA-15** under nitrogen atmosphere.

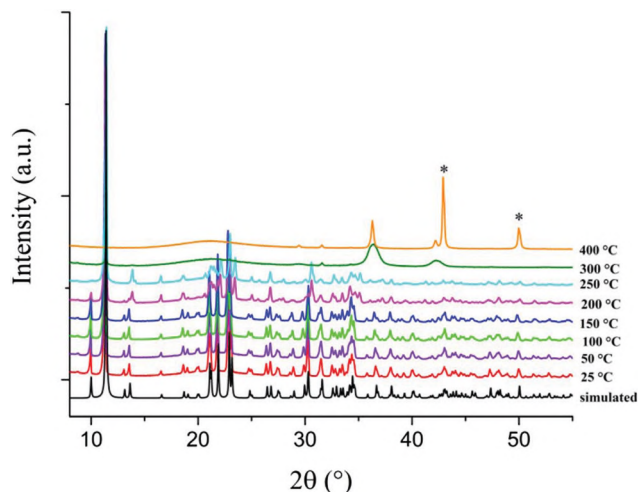


Fig. 4 VTXRPD plots of CFA-15 in the range of 25–400 °C under nitrogen atmosphere. The black line is a simulated XRPD pattern based on single crystal X-ray data. *Peaks belong to Cu phase (PDF no. 4-836).

pattern is consistent with the one calculated from the single crystal structural data (see black curve in Fig. 4). Differences in peak intensities are due to occluded solvent molecules. Variable temperature X-ray powder diffraction studies of CFA-15 are in good agreement with the results from the TGA measurement. The framework is stable up to 150 °C (Fig. 4, dark blue curve). Above this temperature the XRD pattern changes as several peaks disappear and the intensity of the peaks at higher 2θ values decreases, indicating a phase transition due to removal of coordinated DMF molecules. Above 250 °C, the decomposition of the compound is observed and Cu (PDF no. 4-836) is formed as a new crystalline phase at 400 °C.

Activation of CFA-15

After the synthesis, DMF molecules are coordinated to the copper centres in CFA-15. The small weight loss in the TGA curve as well as the first changes in the VTXRPD pattern around 200–250 °C are the first hints that it should be possible to remove the coordinated DMF molecules while the MOF remains crystalline. Especially for further gas sorption experiments, it is necessary to have an activated sample with ideally open pores and free accessible metal centres.

By thermal treatment at 230 °C for 1 h under high vacuum, it is possible to remove the coordinated DMF while the sample remains stable. Activation of the sample leads to a colour change from blue to green (see Fig. 1d) due to changes in the coordination environment of the Cu(II) ions. Thus, the activated CFA-15 exhibits unsaturated and potentially reactive coordination sites.

Characteristic bands in IR spectra that result from coordinated DMF molecules disappear after activation while the other bands remain unchanged (see ESI Fig. S1 and S2†). TG-MS measurement of CFA-15 served as a further proof that coordinated DMF leaved the sample during the activation process.

Removal of the coordinated DMF molecules also leads to differences in XRPD pattern, as some peaks disappear and others are shifted to higher 2θ values. This shift also indicates the flexibility of the framework, as a shift to higher 2θ values implies a reduction of the cell volume due to changes in crystal structure (see ESI Fig. S19†). Due to low crystallinity and relatively small crystal size, it was not possible to characterise the structure of activated CFA-15 via single crystal measurement. Nevertheless, using the DICVOL and TREOR 90 software,²² we were able to determine the possible unit cell parameters of activated CFA-15 from the powder pattern data collected at 250 °C. Both programs determined a quite similar monoclinic cell that shows the following cell parameters: $a = 13.907$ Å, $b = 9.518$ Å, $c = 9.173$ Å, $\beta = 107.36^\circ$, $V = 1159$ Å³ (TREOR, $M_{25} = 11$ $F_{25} = 22$ (0.012171, 97)) and $a = 13.868$ Å, $b = 9.492$ Å, $c = 9.156$ Å, $\beta = 107.31^\circ$, $V = 1151$ Å³ (DICVOL, $M_{20} = 25.2$, $F_{20} = 40.6$ (0.0067, 73)). The space group $C2$ (no. 5) was determined using the EXPO2014 software.²³ Since the same space group and the cell parameters of the activated structure were close to the parameters of CFA-15, the structure of CFA-15 was taken for DFT calculation to obtain crystal model for Rietveld refinement. The refinement of activated CFA-15 was done using the Jana2006 software.²⁴ The Rietveld refinement plot of activated CFA-15 is shown in ESI Fig. S20.† Removal of DMF molecules from the CFA-15 structure leads to contraction of the unit cell (volume change of 46.5 Å³) and decreasing of the unit cell parameters and β -angle. Selected crystal data and details of the structure refinement for activated CFA-15 are collected in Table 2. Fig. 5 shows a portion of the crystal structure of the activated MOF as well as an overlapping of activated CFA-15 and fresh synthesized CFA-15. The crystal data of activated CFA-15 are presented in the ESI (Tables S8–S10†).

Gas sorption measurements

Prior to the measurements, the sample of CFA-15 was washed with DMF and ethanol and heated at 230 °C in high vacuum for one hour to remove occluded and coordinated solvent molecules. Argon as well as nitrogen adsorption isotherms for CFA-15 at 77 K reveal only low BET surface area (~ 90 – 100 m² g^{−1}). However, CO₂ gas sorption measurements on CFA-15 at 194.7 K confirm permanent porosity of the framework and reveal a BET surface area of 340 m² g^{−1}. Due to its smaller kinetic diameter (3.30 Å) and higher measurement temperature (194.7 K), CO₂ can diffuse into the pores of the framework much easier than N₂ or Ar, having a larger kinetic diameter (N₂: 3.64 Å; Ar: 3.40 Å), and lower measuring temperature of 77 K.

The CO₂-sorption isotherms follow type I behaviour, which is characteristic for microporous solids. The maximum uptake achieved at 194.7 K and $p/p_0 = 0.99$ is 63.28 cm³ g^{−1} (Fig. 6), corresponding to a total pore volume of 0.079 cm³ g^{−1}, respectively. The micropore volume of CFA-15 determined at $p/p_0 = 0.2$ is 37 cm³ g^{−1} and the BET surface area determined in the range $p/p_0 = 0.02$ – 0.07 is 340 m² g^{−1}.

MOFs containing coordinatively unsaturated metal centres often represent promising candidates for gas separation, molecular sieving and purification applications. Therefore, the iso-

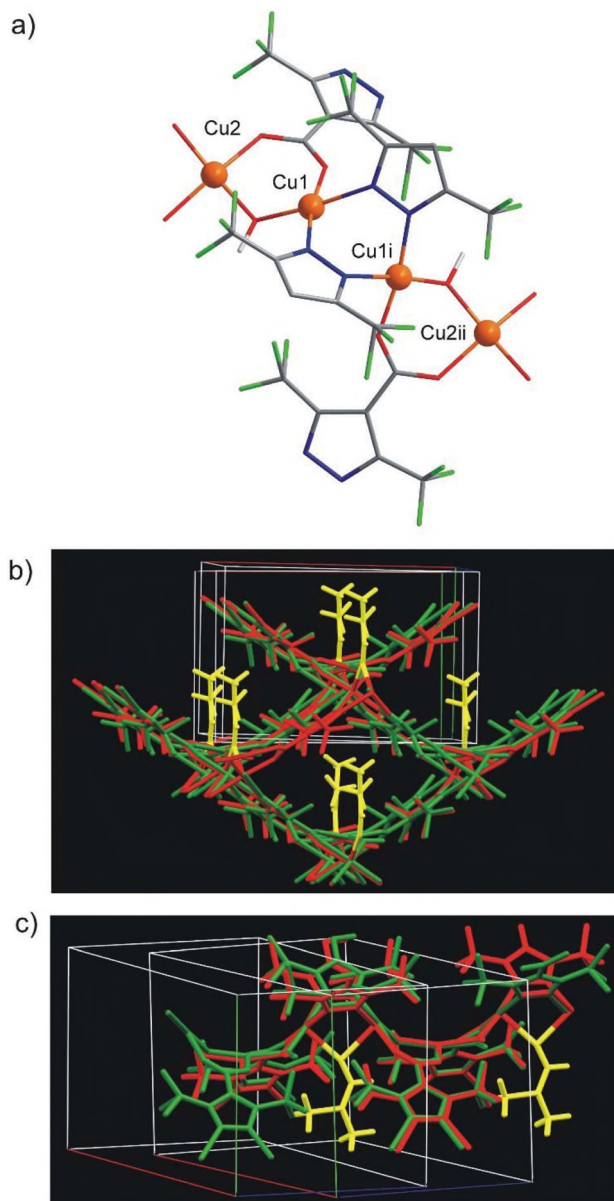


Fig. 5 Portion of the crystal structure of activated **CFA-15** emphasizing coordination of two Cu(II)-centres (a), Cu1i ($1 - x, y, 2 - z$), Cu2ii ($x, y, 1 + z$); (b–c) overlapping of packing diagrams of activated **CFA-15** (green) and **CFA-15** (red) with coordinated DMF molecules (yellow) structures.

steric heats of adsorption of CO, CO₂, O₂ and H₂ in **CFA-15** were determined from adsorption isotherms measured in different temperature ranges (see Fig. 7, Table 1 and ESI Fig. S8–S15†). Typically, the isosteric heats of CO₂ adsorption in MOFs range from 25–35 kJ mol^{−1},²⁵ in exceptional cases a value up to 90–96 kJ mol^{−1} can be reached.²⁶ The heat of adsorption of CO₂ in **CFA-15** reaches a value of 33 kJ mol^{−1}. This value is slightly greater than the value of the heat of sublimation of the adsorbate (26 kJ mol^{−1}).²⁷ The isosteric heat of CO adsorption for **CFA-15** determined from adsorption isotherms measured in the temperature range 183–213 K reaches

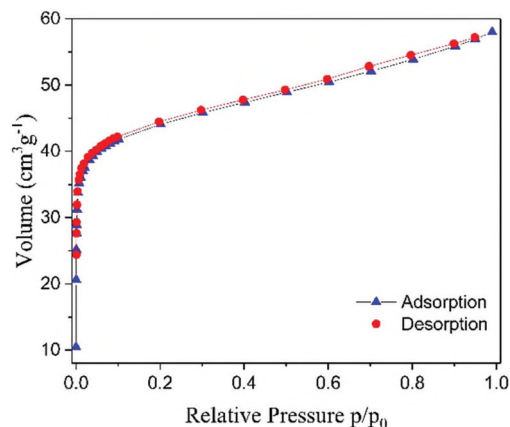


Fig. 6 CO₂ adsorption (blue) and desorption (red) isotherms of **CFA-15** at 194.7 K.

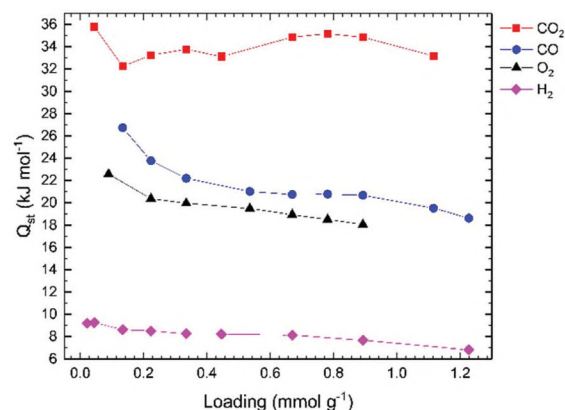


Fig. 7 Isothermic heats of CO (blue), CO₂ (red), H₂ (magenta) and O₂ (black) adsorption in **CFA-15**.

Table 1 Isothermic heats of adsorption of different gases in **CFA-15**

Gas	Temperature range [K]	Isothermic heat low loading [kJ mol ^{−1}]	Isothermic heat higher loading [kJ mol ^{−1}]
CO ₂	273–293	36	33
CO	183–213	27	20
O ₂	183–213	22.5	18
H ₂	97–112	9.2	6.8

a typical physisorption values of 27 kJ mol^{−1} for low loading (<0.15 mmol g^{−1}) and decreases to values of <20 kJ mol^{−1} at high loading. For O₂ and H₂ the measured values of the heat of adsorption with 20 kJ mol^{−1} and 8 kJ mol^{−1} correspond approximately to the values of the heat of sublimation of the adsorbate, and therefore, the interaction is interpreted as physisorption. Typically, the isosteric heat of H₂ adsorption in MOFs ranges from 5–10 kJ mol^{−1} for physisorbed hydrogen.²⁸ If it comes to a formation of metal hydrides, the values normally rise to 15–24 kJ mol^{−1}.²⁹ Especially worth mentioning here is the MOF Cu^I-MFU-4l with isosteric heat of hydro-

Table 2 Crystal data and structure refinement of H₂-tfpc and CFA-15 and activated CFA-15

Compound	H ₂ -tfpc	Cu ^{II} ₃ (tfpc) ₂ (OH) ₂ ·DMF	Cu ^{II} ₃ (tfpc) ₂ (OH) ₂
Empirical formula	C ₆ H ₂ F ₆ N ₂ O ₂	C ₁₅ H ₉ Cu ₃ F ₁₂ N ₅ O ₇	C ₁₂ H ₂ Cu ₃ F ₁₂ N ₄ O ₆
Formula	C ₆ H ₂ F ₆ N ₂ O ₂	Cu ₃ (C ₁₂ F ₁₂ N ₄ O ₄)(O ₂ H ₂)(C ₃ H ₇ NO)	Cu ₃ (C ₁₂ F ₁₂ N ₄ O ₄)(O ₂ H ₂)
<i>M_r</i> /g mol ⁻¹	248.10	789.89	716.8
<i>T</i> /K	200(2)	268	523
Wavelength/Å	0.71073	0.71073	1.5418
Crystal system	Orthorhombic	Monoclinic	Monoclinic
Space group	<i>Cmc</i> 2 ₁ (no. 36)	<i>C</i> 2 (no. 5)	<i>C</i> 2 (no. 5)
<i>a</i> /Å	6.7891(4)	14.2997(4)	13.829(2)
<i>b</i> /Å	6.9057(3)	9.4881(3)	9.462(1)
<i>c</i> /Å	17.1652(9)	9.3862(3)	9.143(1)
β /°	—	109.7120(10)	107.28(1)
<i>V</i> /Å ³	804.76(7)	1198.86(6)	1142.4(3)
<i>Z</i>	4	2	2
<i>D_c</i> /g cm ⁻³	2.048	2.188	2.084
μ /mm ⁻¹	0.240	2.780	4.549
<i>F</i> (000)	488	770	690
θ , (2 θ) range/°	2.373 to 19.942	2.626 to 27.48	5.00 to 70.00
Refls. collected	418	18 173	—
Refls. unique	414	2536	—
<i>R</i> (int)	0.0491	0.0603	—
GooF	1.208	1.147	6.59
Flack parameter	—	0.06(4)	—
<i>R</i> ₁ [<i>I</i> > 2 σ (<i>I</i>)] ^a	0.0668	0.0500	—
<i>wR</i> ₂ (all data) ^b	0.1447	0.1114	—
<i>R</i> _{wp}	—	—	11.97
<i>R</i> _p	—	—	9.41
Largest diff. peak and hole/Å ⁻³	0.338 and -0.406	0.92 and -1.23	—

$$^a R_1 = \sum ||F_o| - |F_c|| / \sum |F_o|, \quad ^b wR_2 = \sum [w(F_o^2 - F_c^2)^2] / \sum [w(F_o^2)^2]^{1/2}.$$

gen chemisorption with values up to 32 kJ mol⁻¹ and O₂ chemisorption up to 53 kJ mol⁻¹.³⁰

Considering the fact that activated **CFA-15** contains coordinatively unsaturated metal sites the experimentally determined heats of adsorption of the different probe gases show unexpectedly low values, approaching values typical of neat physisorption. Therefore, ab initio PW-DFT-D calculations were performed on structural derivatives of **CFA-15**, where the bridging DMF linkers of the original structure have been replaced by different probe gases. (Technical details of the calculations are presented in the ESI†). Dispersion corrected lattice energies have been calculated for fully relaxed 3D periodic models of the primitive cells of activated **CFA-15**, and μ_2 -X @**CFA-15** (μ_2 -X = CO, CO₂, O₂, NO), as well as for the neat probe gases. Sorption energies were then obtained from energy differences according to $\Delta E^{\text{sorp}} = E^{\text{latt}}(\mu_2\text{-X@CFA-15}) - (E^{\text{latt}}(\text{CFA-15}) + E(\text{X}))$. The calculated energy differences ΔE^{sorp} are: -31.5 kJ mol⁻¹ (CO), -34.5 kJ mol⁻¹ (CO₂), -16.5 kJ mol⁻¹ (O₂), and -23.4 kJ mol⁻¹ (NO). The first three calculated values show a very good agreement with experimentally determined heat of adsorption values for the corresponding gases at low loading: -27 kJ mol⁻¹ (CO), -36 kJ mol⁻¹ (CO₂), -22.5 kJ mol⁻¹ (O₂) (cf. Table 1). A closer inspection of the relaxed lattice models of the compounds indicate that the putative bonding interactions of the gas probes (CO, CO₂, O₂) with the open Cu(II) metal sites are predominantly dispersive in nature, which leads to long (non-bonding) Cu(II)-X distances in the calculated lattice models (cf. ESI† for details). It turns out that the

pincer-type arrangement of Cu(II) metal centers in activated **CFA-15** comprising each a square planar coordination environment shows a low propensity to bind gas molecules at their coordinatively unsaturated sites (CUS).

In addition to gas sorption studies, the adsorption of CO₂ in **CFA-15** was studied by diffuse reflectance Fourier-transform IR spectroscopy (DRIFT) to find out whether the adsorption of CO₂ in **CFA-15** is due to physical interactions or because of chemisorption (see Fig. 8 and ESI S3 and S4†). First, the sample was heated up to 120 °C under nitrogen flow (flow: 50 ml min⁻¹). After cooling down to room temperature, a FT-IR spectrum of the activated **CFA-15** was recorded under nitrogen (black curve, Fig. 8). Then, the gas flow was switched to CO₂ (flow: 37 ml min⁻¹) and the temperature was decreased to -70 °C. After 30 minutes, the gas flow was changed to nitrogen again. After flushing the reaction chamber thoroughly, the temperature was gradually increased while recording IR spectra under N₂ at different temperature steps.

In general, the IR spectrum of free CO₂ gas shows two single bands: the ν_3 antisymmetric stretching mode (2349 cm⁻¹) and the ν_2 bending mode (668 cm⁻¹). Adsorption of guest molecules in the pores of a MOF leads to changes in IR spectra. Typically, physisorption of CO₂ causes a red shift of the ν_2 and ν_3 bands as well as a splitting of the ν_2 band. The location of the bands strongly depends on the adsorption position of the gas molecule in the host, ν_3 is usually located between 2328–2368 cm⁻¹, while the splitted ν_2 are between 645–669 cm⁻¹.³¹ Most frequently, CO₂ is bound to the host due

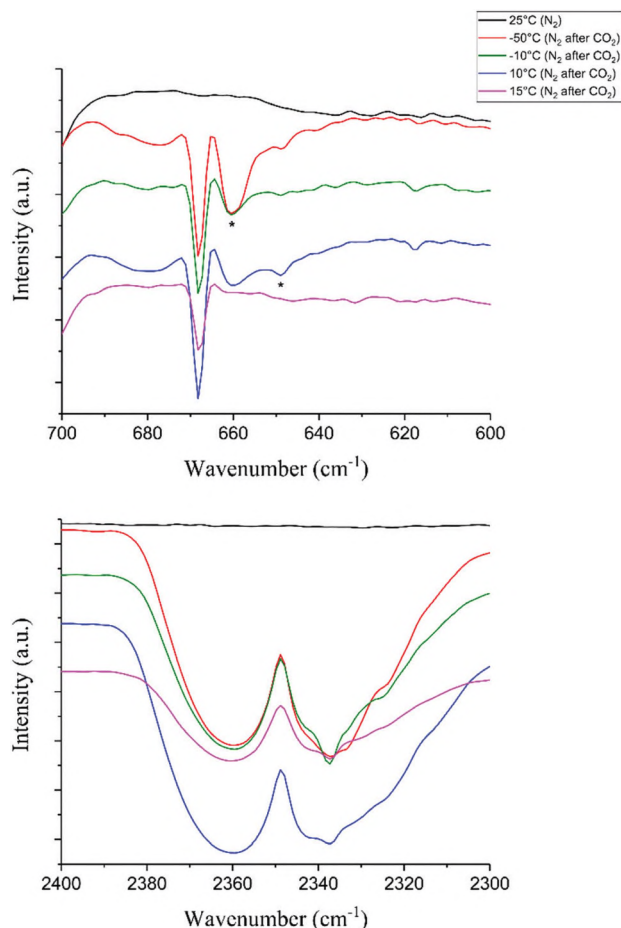


Fig. 8 *In situ* DRIFT spectra of **CFA-15** showing the ν_2 bending region (upper frame) and the ν_3 stretching region (lower frame). The black curve shows the sample under N_2 at room temperature without any CO_2 contact.

to weak non-covalent interactions such as hydrogen bonding, dipole–quadrupole interaction or van der Waals interactions. In Cu-btc, for example, the adsorption of CO_2 to the copper centres causes a shift of ν_3 to 2339 cm^{-1} while ν_2 is shifted to 655 cm^{-1} with a shoulder at 667 cm^{-1} .³² In addition to the non-covalent interactions just mentioned, also the coordination of CO_2 to a Cu(II) centre in several different modes is possible.³³ Furthermore, CO_2 – CO_2 interactions occur due to close intermolecular $O=C=O\cdots C=O_2$ contacts at higher CO_2 -loading. As a consequence, deformation of bond lengths and angles cause a loss of symmetry and therefore further bands/shoulders can arise in the region of the ν_3 antisymmetric stretching mode.³¹

The *in situ* DRIFT spectra of **CFA-15** show bands of the ν_2 bending mode at 660 cm^{-1} and 648 cm^{-1} with a centre around 655 cm^{-1} that is shifted by 12.3 cm^{-1} compared to free CO_2 gas (see Fig. 8, upper frame). This red-shift is enhanced in **CFA-15**, as the Cu(II)-centres are surrounded by coordination partners with strong $-I$ effect due to fluorination of the ligand resulting in further decrease of the electron density at the

metal centre. The ν_3 antisymmetric stretching mode of **CFA-15** is shown in the lower frame of Fig. 8. ν_3 shows a broad band between 2320 – 2350 cm^{-1} with a centre around 2337 cm^{-1} and shoulders at 2342 , 2339 , 2332 and 2323 cm^{-1} . These shoulders could be caused by CO_2 – CO_2 -interactions mentioned above. Additional to the changes in the ν_2 and ν_3 modes, further shifts can be observed (for details see ESI Fig. S4†): $948 \rightarrow 953\text{ cm}^{-1}$, $1590 \rightarrow 1598\text{ cm}^{-1}$, $1550 \rightarrow 1545\text{ cm}^{-1}$, $1506 \rightarrow 1503\text{ cm}^{-1}$ and $1416 \rightarrow 1414\text{ cm}^{-1}$. These bands can be attributed to small changes in the C–H bending vibrations and C=C-stretching vibrations of the aromatic ligand.

Although, apart from the determined high value for the isosteric heat of adsorption for CO_2 , there is no evidence whether the adsorption of CO_2 in **CFA-15** is due to physical interactions or because of chemisorption. It is crucial, however, that the IR-bands resulting from the ν_3 antisymmetric stretching mode as well as the ν_2 bending mode are clearly red-shifted compared to values for free CO_2 gas molecules indicating that CO_2 is strongly adsorbed in the pores of **CFA-15**.

The reversible storage of NO is of great interest for several applications as for example in medicine.³⁴ Reversible binding of NO often poses a challenge, as NO can easily react with traces of H_2O or O_2 leading to the formation of nitrous or nitric acid which subsequently form nitric compounds with the aromatic rings of the ligand. **CFA-15** seems to be a promising candidate for moderately strong binding of NO. There are no positions within the ligand of **CFA-15** that could inadvertently be nitrated. Furthermore, the strong hydrophobicity of **CFA-15** could prevent the disproportionation of NO, therefore, **CFA-15** could find potential application as depot system for NO. In further experiments, the binding of NO to **CFA-15** was investigated and the results are discussed in the following section.

The adsorption of NO in **CFA-15** was studied by diffuse reflectance Fourier-transform IR spectroscopy (see Fig. 9 and ESI Fig. S5 and S6†). First, the sample was heated up to $120\text{ }^\circ\text{C}$

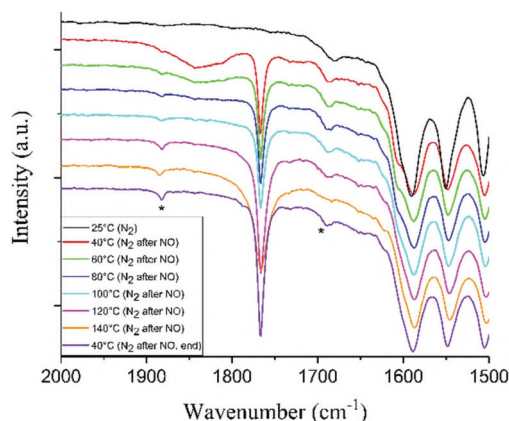


Fig. 9 *In situ* DRIFT spectra of **CFA-15** in the range of 2000 – 1500 cm^{-1} under N_2 after NO treatment at different temperatures. The black curve shows the sample under N_2 at room temperature without any NO contact.

under nitrogen flow (flow: 50 ml min⁻¹). After cooling down to room temperature, a FT-IR spectrum of the activated **CFA-15** was recorded under nitrogen (black curve, Fig. 9). Then, the gas flow was switched to NO (5% NO in Ar) and the temperature was decreased to -140 °C. After 30 minutes, the gas flow was changed to nitrogen again. After flushing the reaction chamber thoroughly, the temperature was gradually increased up to a final temperature of 140 °C while recording IR spectra under N₂ at the different temperature steps. Finally, one last DRIFT spectrum is recorded when the sample is cooled down to 40 °C after heating procedure (purple curve, Fig. 9). The experiment leads to the formation of various new bands in the detected IR-spectra. New bands at 2763, 2450–2400, 1768, 1605, 1435, 1450–1350 and 833 cm⁻¹ can be assigned to accumulating nitrogen oxide (NO₂ and N₂O₄) species, while the bands at 3435 and 2150–2050 cm⁻¹ could be most likely be assigned to reaction products between NO₂/N₂O₄ and the **CFA-15** framework. These listed bands can also be found in similar experiments in literature.³⁵ Unfortunately, we were not able to avoid accumulation of NO₂/N₂O₄ impurities up to now, despite using high-purity (>99.999%) gases. As the amount of MOF used in DRIFT experiments is very low (about 0.1 mg), the presence of trace impurities is already sufficient to observe these side effects. After deduction of the bands mentioned above, two remaining new IR-bands can finally be observed, located at 1882 cm⁻¹ and 1690 cm⁻¹ (marked with * in Fig. 9). Before treating the sample with NO, **CFA-15** already shows a band in the IR spectrum at 1680 cm⁻¹ (black curve). Nevertheless, the band is broader after the experiment showing a shoulder that is shifted to 1690 cm⁻¹, why we expect the formation of a weak but new band at 1690 cm⁻¹ besides the clearly visible new band at 1882 cm⁻¹. Besides the formation of these new bands in IR spectra, also the colour of the sample is a reason to believe in the formation of a stable **NO-CFA-15** complex. During the experiment, the colour of the sample changes from green to brown, indicating a change in the coordination environment of the Cu(II) centres (see picture, ESI Fig. S7†).

In general, gas molecules can be adsorbed in different positions in a host depending on the network structure as well as on the species of the metal centres. NO is often adsorbed in end-on mode to copper centres, while the metal centres value different oxidation states as for example [Cu(III)-NO]⁻, Cu(II)-NO[•] or Cu(I)-NO⁺.³⁶ In structures containing dinuclear hydrogen-bridged copper-units, also the formation of NO₂-[Cu-O-Cu] is observed, where overall two gas molecules are bound.^{36b} The observation of new bands at 1882 and 1690 cm⁻¹ as well as the colour change from green to brown indicate the formation of a new and stable **NO-CFA-15** complex, although there is no evidence in which way the NO is coordinated to the Cu(II) centres. For full investigation of the binding mode, extensive computational studies should be performed.

Photoluminescence and UV-Vis spectroscopy

Solid-state photoluminescence properties of **CFA-15** and the H₂-tfpc ligand were studied at room temperature. H₂-tfpc exhi-

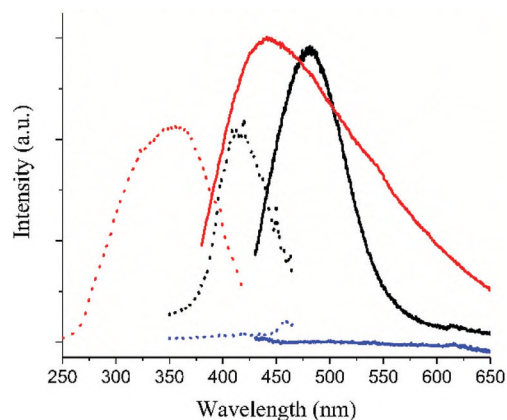


Fig. 10 Solid-state photoluminescence spectra of the H₂-tfpc ligand (red), fresh synthesised **CFA-15** (black) and activated **CFA-15** (blue) at room temperature. Dashed lines: excitation spectra; continuous lines: emission spectra.

bits a broad emission peak under excitation at 360 nm (Fig. 10, red line) and shows maximum emission at 440 nm. The excitation of H₂-tfpc is probably attributed to the $\pi \rightarrow \pi^*$ transition of the aromatic system.³⁷ **CFA-15** shows interesting fluorescence behaviour. Based on their intrinsic paramagnetic properties, Cu(II) centres (d⁹ electron configuration) strongly interrupt the fluorescence of the ligand due to an internal charge transfer resulting in a fluorescence quenching (“turn off fluorescence”). This quenching can also be observed for the activated **CFA-15** sample (Fig. 10, blue line). Interestingly, **CFA-15** with coordinated DMF molecules exhibits a broad emission peak under excitation at 416 nm (Fig. 10, black line) and shows maximum emission at 481 nm. Compared to H₂-tfpc, the emission peak of **CFA-15** is red-shifted. There are many examples in literature with Cu(II), that show so called “turn-on” and “turn-off” fluorescence, when small molecules coordinate to the Cu²⁺ centres.³⁸

The dark blue colour of **CFA-15** crystals is an indication for the presence of Cu(II) centres in the framework structure. In order to confirm the coordination environment of the metal

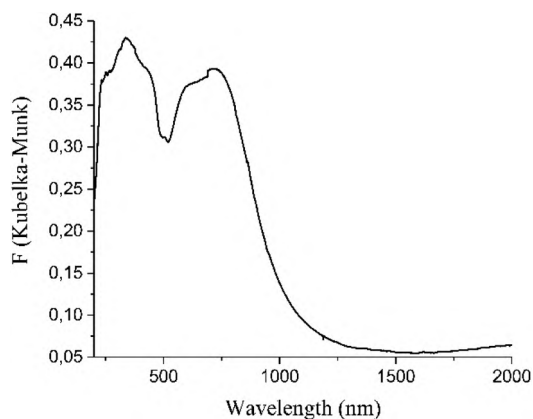


Fig. 11 Solid-state UV-vis spectrum of **CFA-15** at room temperature.

centres, **CFA-15** was analysed by solid-state UV-vis spectroscopy. **CFA-15** shows two strong absorption bands with maxima at 350 nm and 650–750 nm (Fig. 11). The absorption band around 350 nm can either originate from ligand-to-metal charge transfer or from intra-ligand electron transitions. The absorption band at 650–750 nm can be assigned to the d–d transitions of Cu(II) centres. The obtained results are in good agreement with literature data of the Cu(II) MOF HKUST-1 showing similar absorption bands.³⁹

Conclusion

The work reported here describes the synthesis and characterisation of the novel fluorinated metal–organic framework **CFA-15**. **CFA-15** features a non-interpenetrated 3-D microporous structure constructed from 1-D chains of copper(II) ions expanding in the *c*-direction, bridged by OH[−] groups, DMF molecules and tfpc^{2−} ligands. Within the structure of **CFA-15**, two different Cu(II) centres exist, bridging in a {Cu1–Cu1–Cu2–Cu1–Cu2} mode. The framework exhibits hydrophobic rhombic channels running along the crystallographic *c*-axis with apertures of 4.2 Å.

By thermal treatment at 230 °C for 1 h under high vacuum it is possible to remove the coordinated DMF molecules while the sample remains stable. The activated **CFA-15** exhibits coordinatively unsaturated metal centres and a BET surface area of 340 m² g^{−1}. The structure of the activated MOF was refined *via* Rietveld method.

MOFs with unsaturated and reactive metal centres often represent promising candidates for gas separation, molecular sieving and purification applications. Within this work, activated **CFA-15** was tested for several potential applications. **CFA-15** shows the highest binding affinity for CO₂ when directly compared to other small probe gas molecules such as CO, H₂ or O₂. Furthermore, the formation of a **NO@CFA-15** complex was investigated, although there is no complete experimental evidence in which way(s) the NO is coordinated to the Cu(II) centres. To fully characterise the possible different binding modes, far more extensive computational studies would be necessary.

Based on experimental and theoretical gas sorption studies it can be concluded that the square planar d⁹ configuration of Cu(II) metal ions in activated **CFA-15** represents a very stable electronic ground state, preventing adsorbed gas molecules from establishing stable coordinative bonds. The question as to if (or not) this observation can be generalized to structurally similar Cu(II) framework compounds should be of broad interest, since it might be possible to fine-tune the binding characteristic of such dinuclear Cu(II) sites towards specific probe molecules and thus for sensory applications.

Moreover, **CFA-15** shows interesting fluorescence behaviour. While fresh synthesised **CFA-15** exhibits a broad emission band, activation of the MOF leads to a fluorescence quenching. If it is possible to again turn-on the emission of activated **CFA-15** by coordination of small molecules to the unsaturated

metal centres, this MOF could be of great interest for technical application as a sensor material. Also a potential use of **CFA-15** as a filter membrane or as NO-sensor are possible and investigated by our group in further works.

Experimental section

Materials and general methods

All starting materials were of analytical grade and used as obtained from commercial sources without further purification. Thermogravimetric analysis (TGA) was performed with a TGA Q500 analyser in the temperature range of 25–800 °C under nitrogen atmosphere at a heating rate of 5 K min^{−1}. Fourier transform infrared (FTIR) spectra were recorded with an ATR unit in the range of 4000–400 cm^{−1} on a Bruker Equinox 55 FT-IR spectrometer. Diffuse reflectance infrared Fourier-transformed (DRIFT) spectra were recorded with the same instrument equipped with a Harrick Praying Mantis I21012 reaction chamber. Energy-dispersive X-ray spectroscopy (EDX) was performed with a Philips XL-30 scanning electron microscope. Ambient temperature X-ray powder diffraction (XRPD) patterns were recorded on a Seifert XRD 3003 TT diffractometer equipped with a Meteor1D detector operated at 40 kV, 40 mA, Cu Kα ($\lambda = 1.54178$ Å) with a scan speed of 1 s per step and a step size of 0.02° in 2θ . Variable temperature X-ray powder diffraction (VTXRPD) measurements were collected in the 2θ range of 5–60° with 0.02° steps with a Empyrean (PANalytical) Diffractometer equipped with a Bragg-Brentano^{HD} mirror, a PIXcel^{3D} 2 × 2 detector and a XRK 900 Reactor chamber (Anton Paar). The patterns were recorded in a temperature range from 25 to 400 °C, in the 5–50° 2θ range, with one step per 0.4 s, and an angular step width of 0.02° in 2θ . Temperature program between measurements: heating rate (0.5 °C s^{−1}), then 10 min isothermal. All sorption isotherms were measured with a BELSORP-max instrument combined with a BELCryo system. The measurements were performed with CO₂, CO, H₂ and O₂ in the range of $1.00 \times 10^{-4} \leq p/p_0 \leq 1.00$ and in the temperature range of 183–213 K, 273 K–293 K, 97–112 K and 183–213 K, respectively. Luminescence spectra were acquired using a spectrofluorimeter (F9920, Edinburgh Instruments) equipped with a TMS300 monochromator, a S900 single photon photomultiplier, and a Xe 900 450 W xenon arc lamp at r. t. The excitation and emission spectra were corrected for the wavelength-dependent lamp intensity and detector response, respectively. Diffuse reflectance UV-vis-NIR spectra were recorded in the range of 2000–200 nm on a PerkinElmer λ 750s spectrometer equipped with a Labsphere 60 mm RSA ASSY integrating sphere with a 0° d^{−1} measuring geometry. Labsphere Spectralon SRS-99 was used as the white standard.

Synthesis of Cu₃(tfpc)₂(OH)₂·DMF (**CFA-15**)

Copper nitrate trihydrate (30 mg; 0.12 mmol) and H₂-tfpc (25 mg, 0.10 mmol) were dissolved in 1 mL of DMF, 1 mL of EtOH and 1 mL of H₂O, and the solution was placed in a glass

tube (10 mL). The tube was closed and placed in a heating block at 70 °C. After 24 h, the temperature was increased to 85 °C for further 24 h and then cooled to room temperature. The precipitate was filtered, washed with DMF (3 × 2 mL), H₂O (3 × 2 mL) and EtOH (3 × 2 mL), and finally dried at 100 °C under vacuum.

Yield: 19 mg (60%). IR ($\nu(\text{cm}^{-1})$): 3646; 1663; 1589; 1531; 1492; 1439; 1403; 1259; 1216; 1139; 1066; 1024; 947; 830; 809; 729; 696; 672; 573; 554; 466; 445. The IR-spectrum of CFA-15 is shown in ESI (see Fig. S1 and S2†).

Single crystal X-ray crystallography

Single crystal X-ray data were collected on a Bruker D8 Venture diffractometer. Intensity measurements were performed using monochromated (doubly curved silicon crystal) MoK α radiation (0.71073 Å) from a sealed microfocus tube. Generator settings were 50 kV, 1 mA. Data collection temperature was −5 °C for CFA-15 and −74 °C for H₂-tfpc. APEX3 software was used for preliminary determination of the unit cell.⁴⁰ Determination of integrated intensities and unit cell refinement were performed using SAINT.⁴¹ The CFA-15 structure was solved and refined using the Bruker SHELXTL Software Package.⁴² H₂-tfpc was solved by the Intrinsic Phasing routine implemented in APEX3. Both crystal structures were refined using SHELXL.⁴³ Non-hydrogen atoms were refined with anisotropic temperature parameters.

In the case of H₂-tfpc, the crystal structure was solved applying the twin law (1 0 0) (0 1 0) (0 0 −1) −4. Due to this fact, the interatomic distances were restricted using DFIX (O–H and N–H) and SADI (remaining bonds). The anisotropic displacement parameters were also restricted using EADP for atoms in equal bonding situations. Selected crystal data and details of the structure refinement for fresh synthesised CFA-15, activated CFA-15 and H₂-tfpc are provided in Table 2. Complete crystallographic data for the structures reported in this paper as supplementary publication no. CCDC 1906421 (CFA-15), 1946536 (activated CFA-15) and 1913583 (H₂-tfpc).†

Conflicts of interest

There are no conflicts to declare.

Acknowledgements

The authors thank Helena vom Stein for recording the SEM image and Patrizia del Forno for proofreading (both University of Augsburg).

Notes and references

- 1 T.-H. Chen, I. Popov, W. Kaveevivitchai, Y.-C. Chuang, Y.-S. Chen, A. J. Jacobson and O. Š. Miljanič, *Angew. Chem., Int. Ed.*, 2015, **54**, 13902–13906.
- 2 J. H. Yoon, S. B. Choi, Y. J. Oh, M. J. Seo, Y. H. John, T.-B. Lee, D. Kim, S. H. Choi and J. Kim, *Catal. Today*, 2007, **120**, 324–329.
- 3 T.-H. Chen, I. Popov, O. Zenasni, O. Daugulis and O. Š. Miljanič, *Chem. Commun.*, 2013, **49**, 6846–6848.
- 4 (a) C. Yang, X. Wang and M. A. Omary, *J. Am. Chem. Soc.*, 2007, **129**, 15454–15455; (b) C. Serre, *Angew. Chem., Int. Ed.*, 2012, **51**, 6048–6050; (c) K. Peikert, F. Hofmann and M. Fröba, *CrystEngComm*, 2015, **17**, 353–360; (d) C. Yang, U. Kaipa, Q. Z. Mather, X. Wang, V. Nesterov, A. F. Venero and M. A. Omary, *J. Am. Chem. Soc.*, 2011, **133**, 18094–18097.
- 5 (a) P. Pachfule and R. Banerjee, *Encyclopedia of Inorganic and Bioinorganic Chemistry*, John Wiley & Sons, Ltd., 2014, pp. 1–124; (b) S.-I. Noro and T. Nakamura, *NPG Asia Mater.*, 2017, **9**, e433.
- 6 J. Fritzsche, M. Grzywa, D. Denysenko, S. Reschke, K. Sugimoto, H.-A. Krug von Nidda, D. Schmidtner and D. Volkmer, *Dalton Trans.*, 2018, **47**, 12750–12756.
- 7 J. Fritzsche, M. Grzywa, D. Denysenko, V. Bon, I. Senkovska, S. Kaskel and D. Volkmer, *Dalton Trans.*, 2017, **46**, 6745–6755.
- 8 (a) A. Cadiau, K. Adil, P. M. Bhatt, Y. Belmabkhout and M. Eddaoudi, *Science*, 2016, **353**, 137–140; (b) S.-I. Noro, R. Kitaura, M. Kondo, S. Kitagawa, T. Ishii, H. Matsuzaka and M. Yamashita, *J. Am. Chem. Soc.*, 2002, **124**, 2568–2583; (c) S.-I. Noro, S. Kitagawa, M. Kondo and K. Seki, *Angew. Chem., Int. Ed.*, 2000, **39**, 2081–2084; (d) J. B. Decoste, G. W. Peterson, M. W. Smith, C. A. Stone and C. R. Willis, *J. Am. Chem. Soc.*, 2012, **134**, 1486–1489.
- 9 L. Pan, M. B. Sander, X. Huang, J. Li, M. Smith, E. Bittner, B. Bockrath and J. K. Johnson, *J. Am. Chem. Soc.*, 2004, **126**, 1308–1309.
- 10 (a) J. H. Wang, M. Li and D. Li, *Chem. – Eur. J.*, 2014, **20**, 12004–12008; (b) M. Grzywa, C. Geßner, D. Denysenko, B. Bredenkötter, F. Gschwind, K. M. Fromm, W. Nitek, E. Klemm and D. Volkmer, *Dalton Trans.*, 2013, **42**, 6909–6921; (c) C. E. Kivi and D. Song, *Dalton Trans.*, 2016, **45**, 17087–17090; (d) J. P. Zhang and S. Kitagawa, *J. Am. Chem. Soc.*, 2008, **130**, 907–917.
- 11 (a) S. S.-Y. Chui, S. M.-F. Lo, J. P. H. Charmant, A. G. Orpen and I. D. Williams, *Science*, 1999, **283**, 1148–1150; (b) W.-Y. Gao, R. Cai, T. Pham, K. A. Forrest, A. Hogan, P. Nugent, K. Williams, L. Wojtas, R. Luebke, Ł. J. Weseliński, M. J. Zaworotko, B. Space, Y.-S. Chen, M. Eddaoudi, X. Shi and S. Ma, *Chem. Mater.*, 2015, **27**, 2144–2151; (c) N. Zhu, D. Sensharma, P. Wix, M. J. Lennox, T. Düren, W.-Y. Wong and W. Schmitt, *Eur. J. Inorg. Chem.*, 2016, 1939–1943; (d) M. Eddaoudi, J. Kim, J. B. Wachter, H. K. Chae, M. O’Keeffe and O. M. Yaghi, *J. Am. Chem. Soc.*, 2001, **123**, 4368–4369.
- 12 E. Quartapelle Procopio, T. Fukushima, E. Barea, J. A. R. Navarro, S. Horike and S. Kitagawa, *Chem. – Eur. J.*, 2012, **18**, 13117–13125.
- 13 E. Quartapelle Procopio, T. Fukushima, E. Barea, J. A. R. Navarro, S. Horike and S. Kitagawa, *Chem. – Eur. J.*, 2012, **18**, 13117–13125.

- 14 A. Demessence and J. R. Long, *Chem. – Eur. J.*, 2010, **16**, 5902–5908.
- 15 P. Pachfule, Y. Chen, S. Chandra Sahoo, J. Jiang and R. Banerjee, *Chem. Mater.*, 2011, **23**(11), 2908–2916.
- 16 M. Dincă, A. F. Yu and J. R. Long, *J. Am. Chem. Soc.*, 2006, **128**(27), 8904–8913.
- 17 K. Sumida, M. L. Foo, S. Horike and J. R. Long, *Eur. J. Inorg. Chem.*, 2010, 3739–3744.
- 18 I. I. Gerus, R. X. Mironetz, I. S. Kondratov, A. V. Bezdudny, Y. V. Dmytriv, O. V. Shishkin, V. S. Starova, O. A. Zaporozhets, A. A. Tolmachev and P. K. Mykhailiuk, *J. Org. Chem.*, 2012, **77**, 47–56.
- 19 (a) C. López, R. Costa, F. Illas, C. de Graaf, M. M. Turnbull, C. P. Landee, E. Espinosa, I. Mata and E. Molins, *Dalton Trans.*, 2005, 2322–2330; (b) T. N. Sorrell, C. O'Connor, O. P. Anderson and J. H. Reibenspies, *J. Am. Chem. Soc.*, 1985, **107**(14), 4199–4206; (c) C. J. Boxwell, R. Bhalla, L. Cronin, S. S. Turner and P. H. Walton, *J. Chem. Soc., Dalton Trans.*, 1998, 2449–2450.
- 20 (a) L. C. Porter and R. J. Doedens, *Inorg. Chem.*, 1985, **24**(7), 1006–1010; (b) D. B. W. Yawney, J. A. Moreland and R. J. Doedens, *J. Am. Chem. Soc.*, 1973, **95**(4), 1164–1170; (c) S. Meenakumari and A. R. Chakravarty, *Polyhedron*, 1993, **12**(3), 347–349.
- 21 P. Schmieder, D. Denysenko, M. Grzywa, O. Magdysyuk and D. Volkmer, *Dalton Trans.*, 2016, **45**, 13853–13862.
- 22 P.-E. Werner, L. Eriksson and M. Westdahl, *J. Appl. Crystallogr.*, 1985, **18**, 367–370.
- 23 A. Altomare, C. Cuocci, C. Giacovazzo, A. Moliterni, R. Rizzi, N. Corriero and A. Falcicchio, *J. Appl. Crystallogr.*, 2013, **46**, 1231–1235.
- 24 V. Petříček, M. Dušek and L. Palatinus, Crystallographic Computing System JANA2006: General features, *Z. Kristallogr. - Cryst. Mater.*, 2014, **229**(5), 345–352, DOI: 10.1515/zkri-2014-1737. Retrieved 11 Aug. 2019.
- 25 K. Sumida, D. L. Rogow, J. A. Mason, T. M. McDonald, E. D. Bloch, Z. R. Herm, T.-H. Bae and J. R. Long, *Chem. Rev.*, 2012, **112**(2), 724–781.
- 26 (a) A. Demessence, D. M. D'Alessandro, M. L. Foo and J. R. Long, *J. Am. Chem. Soc.*, 2009, **131**, 8784–8786; (b) T. M. McDonald, D. M. D'Alessandro, R. Krishna and J. R. Long, *Chem. Sci.*, 2011, **2**, 2022–2028.
- 27 (a) <https://webbook.nist.gov/cgi/cbook.cgi?ID=C124389&Mask=4>; (b) J. A. Dunne, M. Rao, S. Sircar, R. J. Gorte and A. L. Myers, *Langmuir*, 1996, **12**, 5896–5904.
- 28 Y.-S. Bae and R. Q. Snurr, *Microporous Mesoporous Mater.*, 2010, **132**, 300–303.
- 29 L. Schlaphbach and A. Züttel, *Nature*, 2001, **414**, 353–358.
- 30 D. Denysenko, M. Grzywa, J. Jelic, K. Reuter and D. Volkmer, *Angew. Chem., Int. Ed.*, 2014, **53**, 5832–5836.
- 31 K. L. Kauffman, J. T. Culp, A. Goodman and C. Matranga, *J. Phys. Chem. C*, 2011, **115**, 1857–1866.
- 32 P. La Manna, I. Di Giambattista, A. Brasiello, G. Scherillo, P. Musto and G. Mensitieri, *Chem. Eng. Trans.*, 2017, **57**, 1165–1170.
- 33 D. Kim, J. Park, Y. S. Kim and M. S. Lah, *Sci. Rep.*, 2017, **7**, 41447.
- 34 (a) S. R. Miller, E. Alvarez, L. Fradcourt, T. Devic, S. Wuttke, P. S. Wheatley, N. Steunou, C. Bonhomme, C. Gervais, D. Laurencien, R. E. Morris, A. Vimont, M. Daturi, P. Horcajada and C. Serre, *Chem. Commun.*, 2013, **49**, 7773–7775; (b) J. L. Harding and M. M. Reynolds, *J. Am. Chem. Soc.*, 2012, **134**(7), 3330–3333; (c) A. R. Butler and D. L. H. Williams, *Chem. Soc. Rev.*, 1993, **22**, 233–241; (d) H. Zhu, B. Ka and F. Murad, *World J. Surg.*, 2007, **31**, 624–631; (e) T. Yang, A. N. Zelikin and R. Chandrawati, *Adv. Sci.*, 2018, **5**, 1701043.
- 35 D. Denysenko and D. Volkmer, *Faraday Discuss.*, 2017, **201**, 101–112.
- 36 (a) M. Sarma and B. Mondal, *Inorg. Chem.*, 2011, **50**, 3206–3212; (b) A. M. Wright, G. Wu and T. W. Hayton, *J. Am. Chem. Soc.*, 2010, **132**, 14336–14337; (c) T. Nobuko and X. Qiang, *Bull. Chem. Soc. Jpn.*, 2002, **75**, 1861–1862; (d) P. Concepción, M. Boronat, R. Millán, M. Moliner and A. Corma, *Top. Catal.*, 2017, **60**, 1653–1663; (e) R. Zhang, J.-S. McEwen, M. Kollár, F. Gao, Y. Wang, J. Szanyi and C. H. F. Peden, *ACS Catal.*, 2014, **4**, 4093–4105.
- 37 J. Fritzsche, D. Denysenko, M. Grzywa and D. Volkmer, *Dalton Trans.*, 2017, **46**, 14907–14915.
- 38 (a) X.-Y. Xu, Q.-C. Chen, Y.-D. Yu and X.-C. Huang, *Inorg. Chem.*, 2015, **55**, 75–82; (b) K. Shankar and J. B. Baruah, *ChemistrySelect*, 2016, **1**, 3038–3044; (c) J. Ferrando-Soria, H. Khajavi, P. Serra-Crespo, J. Gascon, F. Kapteijn, M. Julve, F. Lloret, J. Pasán, C. Ruiz-Pérez, Y. Journaux and E. Pardo, *Adv. Mater.*, 2012, **24**, 5625–5629; (d) X. Zhu, H. Zheng, X. Wei, Z. Lin, L. Guo, B. Qiu and G. Chen, *Chem. Commun.*, 2013, **49**, 1276–1278; (e) D. Maheshwaran, T. Nagendraraj, P. Manimaran, B. Ashokkumar, M. Kumar and R. Mayilmurugan, *Eur. J. Inorg. Chem.*, 2017, 1007–1016.
- 39 (a) C. Prestipino, L. Regli, J. G. Vitillo, F. Bonino, A. Damin, C. Lamberti, A. Zeccina, P. L. Solari, K. O. Kongshaug and S. Bordiga, *Chem. Mater.*, 2006, **18**, 1337–1346; (b) H. K. Kim, W. S. Yun, M.-B. Kim, J. Y. Kim, Y.-S. Bae, J. Lee and N. C. Jeong, *J. Am. Chem. Soc.*, 2015, **137**, 10009–10015.
- 40 APEX3 Version 2016.9 ed, Bruker AXS Inc., 2016.
- 41 SAINT Version 8.37A ed, Bruker AXS Inc., 2015.
- 42 XL Version 2013/3; G. M. Sheldrick, *Acta Crystallogr., Sect. A: Found. Crystallogr.*, 2008, **64**, 112.
- 43 G. M. Sheldrick, *Acta Crystallogr., Sect. C: Struct. Chem.*, 2015, **71**, 3–8.